Corrosion Studies on Post-Weld Heat Treated Dissimilar AISI 2205 and AISI 310 Joints Using Electrochemical Noise Analysis

Mahadevan Govindasamy ✉ – Lloyd Jenner Mangalakaran Joseph Manuel – Senthilkumar Thamilkolunthu
Department of Mechanical Engineering, University College of Engineering, Anna University, India
✉ gmahadevan80@aubit.edu.in

Abstract *The corrosion behavior of dissimilar weldments between AISI310 and AISI2205 stainless steels in a 5 % calcium chloride solution at 50 °C was investigated under three conditions: as-welded, lower post-weld heat treatment at 800 °C, and higher post-weld heat treatment at 1000 °C. Microstructural examination revealed severe pitting in the as-welded sample, with pit widths ranging from 270 µm to 360 µm. The lower heat-treated sample had larger pits (310 µm to 370 µm), while the higher heat-treated sample showed homogeneous corrosion with a protective oxide coating. The as-welded sample had the highest corrosion rate, followed by the lower heat-treated sample, which had a moderate rate, and the higher heat-treated sample had the lowest rate. The corrosion current densities were 5.26×10^{-3} mA/cm², 4.6×10^{-4} mA/cm², and 1.4×10^{-4} mA/cm², respectively. Electrochemical noise measurements confirmed these findings, with the higher heat-treated sample showing negligible localized corrosion and homogenous corrosion behavior.*

Keywords *AISI2205, AISI310, corrosion, electrochemical impedance spectroscopy, $CaCl_2$*

Highlights:

- *Dissimilar AISI2205 and AISI310 joints were subjected to post weld heat treatment (PWHT) for improving its corrosion resistance.*
- *PWHT improved the corrosion characteristics of the dissimilar joints.*
- *Electrochemical noise evaluation revealed that noise intensity was lower in higher temperature PWHT 1000 °C than other joints.*

1 INTRODUCTION

The requirement for advanced engineering applications requires high-performance materials, often requiring welding of incompatible metals. Dissimilar stainless steel welding is particularly notable for its combined benefits of corrosion resistance, mechanical strength, and cost-effectiveness [1] and [2]. AISI 2205 duplex stainless steel and AISI 310 austenitic stainless steel are frequently used in industries such as chemical processing, oil and gas, and marine environments [3] and [4]. This combination leverages the high strength and weldability of duplex stainless steel with the high-temperature resistance of austenitic steel [5]. However, welding different stainless steels poses challenges, particularly regarding corrosion behavior, which affects the durability of welded structures in chloride-rich environments [6]. Welding can alter the microstructure at the weld junction, leading to variations in corrosion resistance [7]. Issues like residual stresses, phase transitions, and microstructural heterogeneities near the weld interface can become sites for localized corrosion, compromising joint integrity [8]. Research on corrosion in stainless steel welds focuses on factors like welding procedures, filler materials, and environmental conditions [9]. Galvanic corrosion, driven by the electrochemical potential difference between base metals, is a primary concern in dissimilar welds [10]. The corrosion behavior is significantly influenced by welding process parameters and post-weld heat treatment (PWHT) [11]. Calcium chloride ($CaCl_2$) solution is often studied for its resemblance to industrial chloride-rich conditions, which promote pitting and crevice corrosion in stainless steels [12] and [13]. PWHT mitigates the adverse effects of welding by relieving residual stresses and homogenizing the microstructure [14] and [15]. Methods such as high- and low-temperature treatments each affect the welded joint's properties differently [16]. Proper PWHT parameters can significantly enhance the corrosion resistance of dissimilar welds in harsh chloride environments [17]. This study evaluates the corrosion resistance of AISI2205-AISI310 dissimilar joints subjected to PWHT at two temperatures, using electrochemical techniques to monitor corrosion behavior in 5 % aqueous calcium chloride over 12 days.

2 MATERIALS & METHODS

2.1 Material Preparation and Welding

The base materials used in this research were AISI 310 stainless steel (SS) and AISI 2205 duplex stainless steel (DSS), both acquired from Kheteshwar Metals, Mumbai, India, as rolled sheets with a thickness of 5 mm. Selecting the right filler wire is crucial for achieving optimal joint quality. ER2205 filler wire is particularly sought after due to its lower ferrite content, which demonstrably improves weldability [18]. As a better option, 2.6 mm ER2205 filler wire was chosen for conducting welding studies. The chemical aspects of both the base material (BM) and filler wire were determined by using spark spectrometer. Sparks were ignited at various regions, and the elemental composition was subsequently recorded. The BMs were sectioned into rectangular pieces measuring 150 mm in length and 100 mm in width using abrasive cutting machine, and the edges were then properly ground. Then, the cut pieces underwent a thorough cleaning process for removing any dirt, oil, or impurities. The welding process was done using a single V-butt joint configuration. According to ASTM E8M 04 standards [19], V-shaped grooves were prepared with a 40º angle and a root gap of 1.2 mm [20].

A dual shielding gas controller and a customized GTAW welding setup were used for fabrication of the joints. A 2.4 mm diameter, 2 % thoriated tungsten electrode that was positioned at a 45° angle was used for the welding tests. The shielding gas was directed by a (12.2 mm internal diameter) nozzle that was positioned 5 mm distance. An electronic gas management unit was designed so that shielding gases could be switched between. Two timing circuits, one for each solenoid valve regulating the gases, were present in this machine. To maintain a balanced 50 % duty cycle, both gases were supplied at equal flow rates but alternated at regular intervals. Based on the reported literatures [21] and [22] and trial experiments, specific technological parameters for the welding experiments were selected and are detailed in Table 1.

Table 1. Designation of joints, welding parameters and heat treatment details

Joint	AISI310-AISI2205		
Designation	As-welded	LPWHT	HPWHT
Ageing temperature [°C]	-	800	1000
Welding current [A]	90 to 120	90 to 120	90 to 120
Welding voltage [V]	14 to 18	14 to 18	14 to 18
Welding speed [mm/s]	3.5	3.5	3.5
Gas flow rate [l/min]	8	8	8

After joining AISI310 SS with AISI2205 DSS, the specimens underwent PWHT. The dissimilar welds were heated for 90 minutes at two aging temperatures, namely 800 °C at lower post-weld heat treatment (LPWHT) and 1000 °C at higher post-weld heat treatment (HPWHT), and subsequently quenched in water. Three sets of joints were subjected to heat treatment, while one set was left untreated for comparative analysis. The designations for the heat-treated joints and information regarding aging temperatures are shown in Table 1.

2.2 Studies on Corrosion Characteristics

Aqueous calcium chloride with a concentration of 5 % was used to create the caustic solution. To conduct each experiment, 100 ml of corrosive solution was added to an open flask and heated to 55 ºC using an electrical heater. AISI2205-AISI310 dissimilar joints in as-welded, LPWHT and HPWHT conditions were used to make the electrodes. After being cut to the dimensions of 10 mm × 5 mm × 2 mm, the samples for the electrochemical procedures were polished using silicon carbide paper, rinsed with distilled water, cleaned with acetone, and dried in a warm air stream. For the electrical connection, the specimens were spot-welded to a 150 mm long, 1 mm diameter 80.0Cr-20.0Ni wire. This wire was then separated from the corrosive solution by enclosing it in glass tubes and filling the gap between

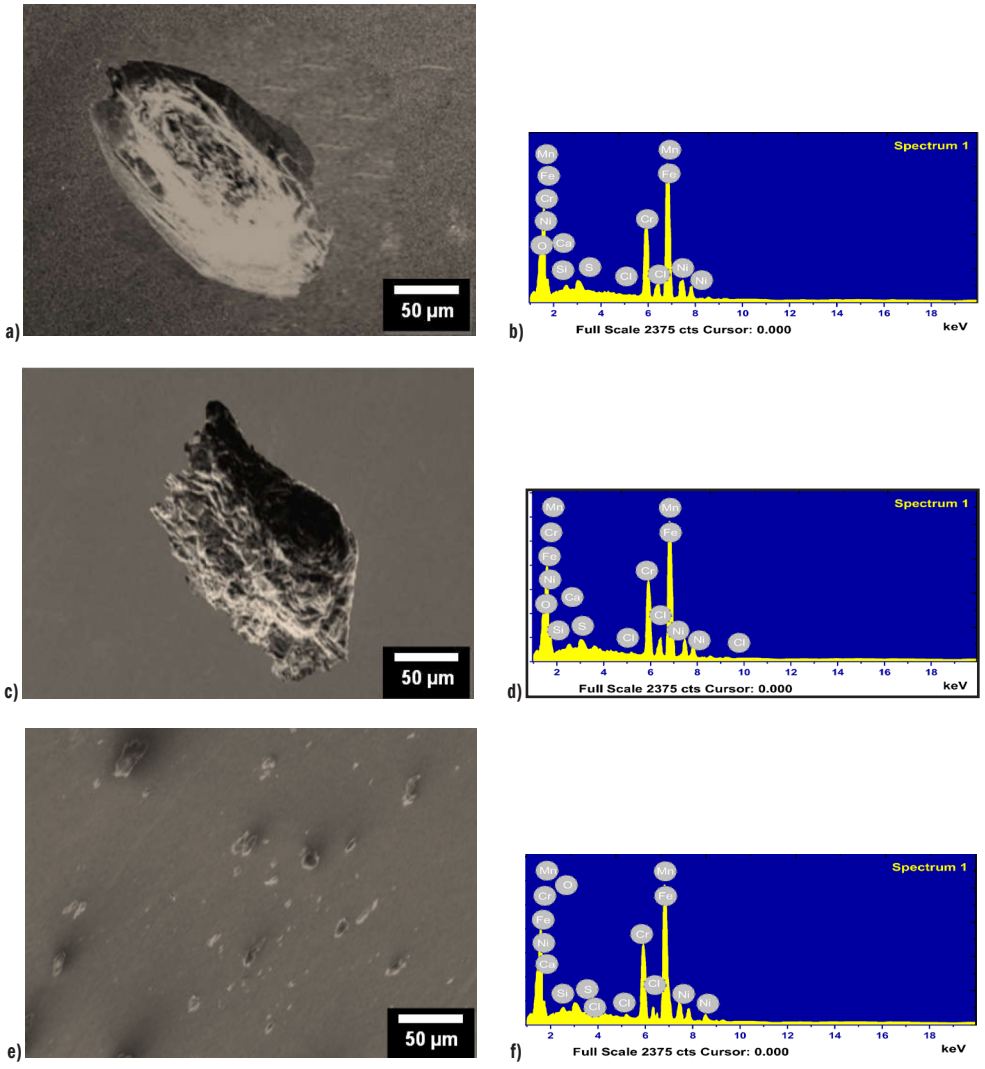

Fig. 1. Micrographs and EDX analysis of dissimilar AISI310-AISI2205 samples exposed to an aqueous $CaCl_2$ solution: a) SEM as-welded sample, b) ADYX as welded sample in the as-welded condition, c) SEM – LPWHT sample, d) EDAX – LPWHT sample, e) SEM – HPWHT sample, and f) EDAX – HPWHT sample

the glass tubes and the electrical connecting wire with refractory silicon. Applying over-potential with a sweep rate of 1 mV/s, ranging from –400 mV below to 800.0 mV above the corrosion potential, the polarization curves were developed [23] and [24].

The electrochemical cell consisted of working electrodes (as-welded, PWHT1, PWHT2), a reference electrode (Ag/AgCl), and an auxiliary electrode (platinum wire). Electrochemical potential and current noise measurements were carried out using a three 'identical' electrode configuration, with one reading per second to compile records of 1024 points every four hours for 12 days. All three electrochemical procedures were performed with an ACM Gill 8AC potentiostat accurately controlled by a personal computer. For qualitative examination, the surface morphology of the corroded specimens was investigated using scanning electron microscopy (SEM) in conjunction with energy dispersive X-ray analysis (EDAX). The SEM examination was carried out utilizing the JEOL JSM-6490LV microscope.

3 RESULTS AND DISCUSSION

3.1 SEM-EDX Analysis

SEM-EDX images of the three corroded dissimilar AISI2250-AISI310 joints (as-welded, LPWHT & HPWHT) which underwent corrosion in CaCl2 solution are shown in Fig. 1a and b, Fig. 1c and d and Fig. 1e and f, respectively.

According to the SEM with EDX examination, the three types of welded samples exhibit diverse corrosion behaviors. The as-welded sample exhibited heavily corroded surface with pits ranging from 270 µm to 360 µm in diameter. EDX analysis found chloride species, indicating that chromium and iron were selectively dissolved, most likely as chlorides. This mixed corrosion process shows localized pitting and general degradation, which are characteristic of untreated weld joints exposed to chloride [25]. The LPWHT sample indicated a morphology similar to the as-welded condition, but with slightly larger pits (310 µm to 370 µm). This indicated that, while LPWHT at 800 °C was intended to relieve tensions and polish the microstructure, it was not completely efficient in preventing the beginning of localized pitting corrosion, particularly in chloride environments. Localized pitting and similar elemental trends reported in both LPWHT and as-welded samples lend support to this theory. The HPWHT sample exhibited an evenly corroded surface with no pits. EDX examination revealed the creation of a protective oxide layer predominantly formed of chromium and iron oxides, with nickel and manganese present in trace levels [26]. Surface ruptures occur in as-welded samples because there is no persistent oxide layer, resulting in localized pitting and selective dissolving of alloy components such as chromium and iron. This makes the surface susceptible to hostile substances such as chlorides. In HPWHT samples, high-temperature treatment promotes the creation of a homogeneous and protective oxide layer, predominantly composed of chromium and iron oxides, which greatly lowers surface deterioration and the risk of localized corrosion. This homogeneous corrosion pattern, together with the existence of a persistent oxide layer, suggests that HPWHT at 1000 °C effectively reduces localized corrosion, offering increased resistance to chloride-induced pitting [27].

3.2 Polarization Curves

Fig. 2 presents the polarization curves of AISI310-AISI2250 at as-welded, LPWHT and HPWHT conditions. The parameters of potentiodynamic polarization curves of dissimilar joints AISI2205-AISI310 with different PWHT conditions exposed in the corrosive solution are shown in Table 2. At higher temperatures, the as-welded, LPWHT, and HPWHT samples behaved differently, according to the corrosion characteristics (Table 2).

Table 2. Parameters of potentiodynamic polarization curves of dissimilar joints AISI2205-AISI310 with different PWHT conditions exposed in the corrosive solution

	AISI2205-AISI310 dissimilar joint	AISI2205-AISI310	AISI2205-AISI310
Condition	As-welded	LPWHT	HPWHT
β_a [mV/decade]	304.7	291.2	134.6
β_c [mV/decade]	71.2	99.6	51.3
E_{corr} [mV]	231.3	–14.8	56.9
I_{corr} [mA/cm^2]	5.26×10^{-3} mA/cm^2	4.6×10^{-4} mA/cm^2	1.4×10^{-4} mA/cm^2

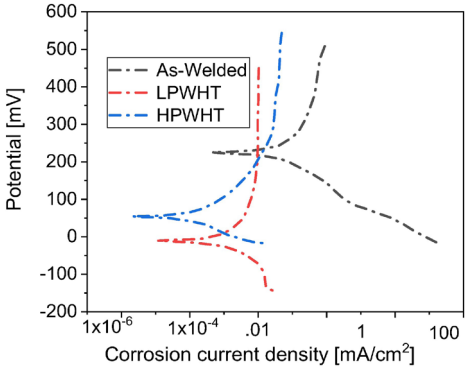

Fig. 2. Polarization curves of AISI310-AISI2250 at as-welded, LPWHT and HPWHT

The as-welded sample had the maximum corrosion rate ($\beta_a = 304.7$ mV/decade, $\beta_c = 71.2$ mV/decade). The corrosion potential E_{corr} was measured at 231.3 mV, and the corrosion current density I_{corr} was 5.55×10^{-3} mA/cm², suggesting maximal susceptibility. Corrosion potential (E_{corr}) denotes a material's ability to corrode; a lower E_{corr} indicates greater susceptibility. Corrosion current density (I_{corr}) indicates the rate of material degradation. Higher I_{corr} values, as seen in the as-welded sample, indicate faster corrosion and a greater sensitivity to corrosion in severe conditions. In comparison to the as-welded sample, the LPWHT sample demonstrated a moderate improvement in corrosion resistance. With β_a at 291.2 mV/decade and β_c at 99.6 mV/decade, the corrosion potential E_{corr} was found to be –14.8 mV.

The corrosion current density was 4.71×10^{-4} mA/cm² (I_{corr}), indicating a medium corrosion rate. Among the samples tested, sample C (HPWHT) exhibited the superior resistance to corrosion. This was evident by its lowest Tafel slopes (β_a at 134.6 mV/decade and β_c at 51.3 mV/decade). Additionally, it had the lowest corrosion potential (E_{corr} at 56.9 mV) and current density (I_{corr} at 1.45×10^{-4} mA/cm²), signifying minimal corrosion susceptibility.

3.3 Electrochemical Noise Measurements

Fig. 3 presents the current and potential time series at 55 ºC for as-welded, LPWHT and HPWHT. These data were used for showing the major localized corrosion activity, taking into account the three typical forms of electrochemical noise generated by different types of corrosion processes [28]:

a. Type I (Pitting): Consist of transients of high intensity with a high repetition rate. This type of corrosion is often characterized by the sudden appearance of small holes or pits in the metal surface.

b. Type II (Mixed): It is a combination of transients of type I and oscillations of short amplitude. This type of corrosion suggests a combination of localized pitting and a more general attack on the metal surface.
c. Type III (Uniform): The pattern noise is formed by oscillations of low amplitude. This type of corrosion refers to a gradual and relatively even attack on the entire exposed metal surface.

The as-welded specimens exhibited the highest corrosion rate, indicated by significantly higher current density values compared to LPWHT and HPWHT. As-welded specimens generally showed potential and current time series with random oscillations of extremely low intensity, resembling those observed at LPWHT & HPWHT. In comparison to LPWHT & HPWHT samples, the potential noise for as-welded specimens showed a greater range, roughly 118 mV, suggesting a nobler nature. This is consistent with the distinct way that the $CaCl_2$ corrosion system responds to heat treatment and lines up with the behavior shown in the polarization curves. LPWHT sample's current and potential time series showed a clear noise pattern with noticeable transients and oscillatory behavior. In electrochemical noise studies, oscillatory behavior in LPWHT samples showed occasional breakdown and recovery of the passive oxide layer caused by localized pitting corrosion [29]. This indicated increased activity, especially on 5th and 6th day, which was compatible with localized corrosion or the breakdown and recovery

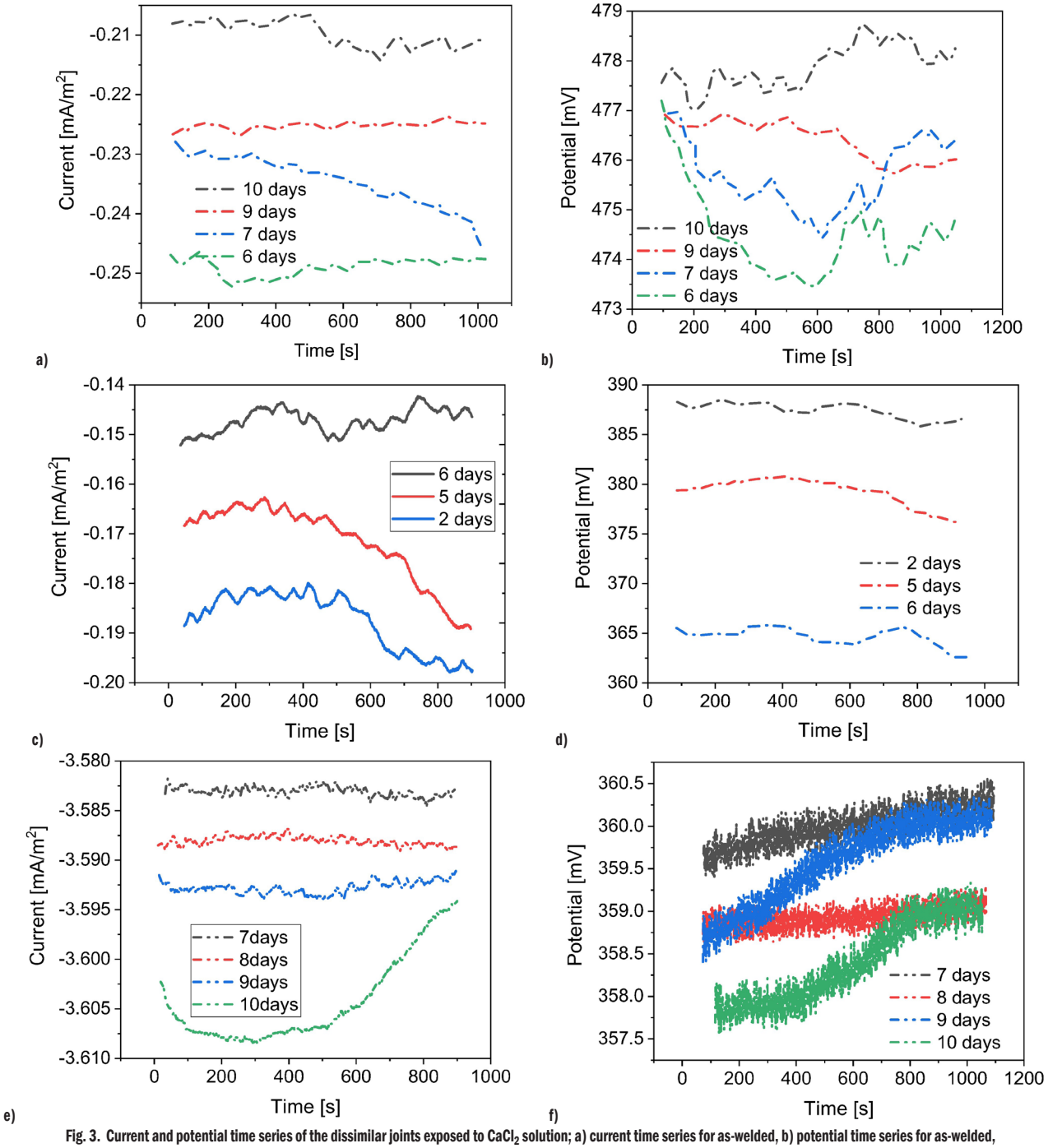

Fig. 3. Current and potential time series of the dissimilar joints exposed to $CaCl_2$ solution; a) current time series for as-welded, b) potential time series for as-welded, c) current time series for LPWHT, d) potential time series for LPWHT, e) current time series for HPWHT, and f) potential time series for HPWHT

of the passive film. Interestingly, the transient activity that was seen on those days did not persist for the duration of the experiment, suggesting that the process was localized and only took place on those days. It is possible to interpret the notable transients seen on those two days as the rupture of the passive oxide coating or localized corrosion events because they were marked by abrupt current rises, potential decreases, and recovery. The rupture of the passive oxide coating in LPWHT samples happens when the protective film that typically protects the metal from corrosion becomes unstable due to localized pressures, impurities, or environmental conditions. This disintegration exposes the underlying metal to corrosive chemicals, which accelerates localized corrosion. Factors such as chloride ions, temperature variations, and mechanical stressors can all weaken the oxide layer and cause it to break. Once the protective coating is compromised, corrosion accelerates until the oxide layer reforms or stabilizes [30].

Even though these transients were noticeable on those two days, the remaining time series showed low-amplitude random oscillations that might have contributed to the localised activity in addition to a mixed corrosion process [31]. This aligned with the findings from the SEM analysis, indicating both techniques identified the susceptibility of AISI2205-AISI310 joints to a combination of localized and mixed corrosion processes. HPWHT showed no notable anodic or cathodic transients in the current and potential time series, in line with the as-welded condition. For HPWHT, the current density stayed negative and extremely low, indicating a low expected rate of corrosion. The cathode electrode's preferential dissolution was indicated by the negative values, which essentially reversed the direction of the current. The present time series indicated low-amplitude random oscillations without any notable anodic transients and just two notable cathodic transients that would indicate the metallic oxide film recovering [32]. As-welded specimens displayed markedly higher current densities than PWHT2, indicating accelerated corrosion rates with rising temperature, a characteristic observed in the $CaCl_2$ corrosion system as reported in previous studies [33].

3.4 Localization Index

The localization index (LI) was computed in order to measure the correlation between the electrochemical noise signals and the corrosion process. Localized corrosion activity is shown by *LI*, which is the ratio of the current noise standard deviation (σ_i) to the root-mean-square current value (I_{rms}). The range of *LI* values, typically between 0 and 1, is taken into account in the study. *LI* approaches 1 for current fluctuations that are noticeably greater than the mean current. On the other hand, *LI* values near 0 suggest that current fluctuations are negligible in relation to the mean current [34].

Localization index of AISI2205-AISI310 dissimilar joints exposed to $CaCl_2$ at different PWHT conditions are shown in Fig. 4. Throughout the experiment, *LI* values were computed from each time series record derived from the electrochemical noise measurements. Values for the localization index were primarily found in the interval between the uniform and mixed corrosion zones. The mixed corrosion zone was primarily where the *LI* of the as-welded sample was located. This observation was consistent with multiple transients being present in the electrochemical noise pattern, indicating a combination of more widespread corrosion processes and localized assault. Multiple transients in the *LI* show the presence of various corrosion mechanisms, including both localized and uniform corrosion processes. This indicates that the electrochemical environment is unstable, with fast swings in corrosion activity resulting in pitting and general degradation, which is typical of mixed corrosion behavior [35]. SEM data, which show a greater vulnerability to localized corrosion attack, supported this observation.

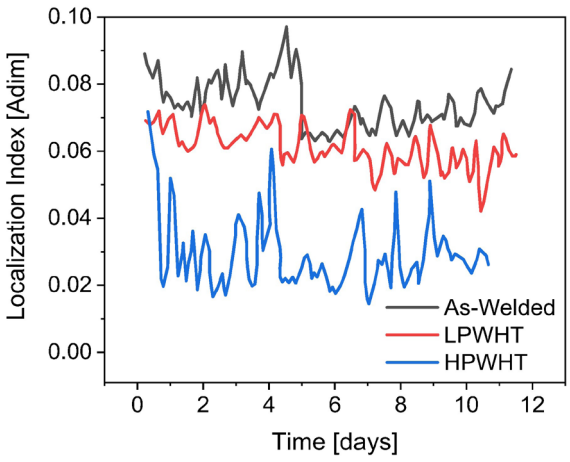

Fig. 4. Localization index (dimensionless) of AISI2205-AISI-310 dissimilar joints exposed to CaCl2 at different PWHT conditions

The LPWHT sample exhibited *LI* values positioned near the border between uniform and mixed corrosion zones. This suggested an intermediate behavior, where localized corrosion was less pronounced compared to the as-welded condition. In mixed corrosion zones, intermediate behavior in LPWHT samples results from partial stabilization of the passive oxide layer, which reduces the severity of localized corrosion when compared to as-welded samples. This results in less noticeable pitting while yet allowing for some localized attack, showing a balance of uniform and localized corrosion processes [36] and [37]. This might be attributed to the absence of significant transients in the corresponding electrochemical noise data, potentially indicating a reduction in localized activity due to the low-temperature post-weld heat treatment. In contrast, the HPWHT sample maintained the *LI* firmly within the uniform or generalized corrosion zone. This consistency aligned with the minimal transients observed in the electrochemical noise pattern, suggesting a predominantly uniform corrosion process [38].

4 CONCLUSIONS

The corrosion performance of post-weld heat-treated AISI2205-AISI310 dissimilar stainless steel joints exposed to a 5 % $CaCl_2$ solution for twelve days was investigated experimentally. The study incorporated SEM analysis alongside polarization curves, electrochemical noise data, and electrochemical impedance plots. According to the results, LPWHT joints and as-welded joints displayed a mixed corrosion process, while HPWHT joints (treated at 1000 ºC) displayed a uniform corrosion process. HPWHT joints had noise signals with a low amplitude and high-frequency pattern, according to electrochemical noise analysis, which coincided with the uniform corrosion that was seen visually. As-welded and LPWHT joints, on the other hand, showed many medium-intensity transients, indicating a more intricate corrosion process. A helpful indicator of corrosion localization was produced by the localization index parameter, which matched the visual observations of the corroded samples quite well.

REFERENCES

[1] Maurya, A.K., Pandey, C., Chhibber, R. Dissimilar welding of duplex stainless steel with Ni alloys: A review. *Int J Press Vessels Pip* 192 104439, (2021) **DOI:10.1016/j.ijpvp.2021.104439**

[2] Verma, J., Taiwade, R.V. Effect of welding processes and conditions on the microstructure, mechanical properties and corrosion resistance of duplex stainless steel weldments-A review. *J Manuf Process* 25 134-152 (2017) **DOI:10.1016/j.jmapro.2016.11.003**

[3] Zhu, P., Cao, X., Wang, W., Zhao, J., Lu, Y., Shoji, T. (2017). An investigation on microstructure and pitting corrosion behavior of 316L stainless steel weld joint. *J Mater Res* 32 3904-3911 **DOI:10.1557/jmr.2017.316**

[4] Xiong, J., Tan, M.Y., Forsyth, M. The corrosion behaviors of stainless steel weldments in sodium chloride solution observed using a novel electrochemical measurement approach. *Desalination*, 327 39-45, (2013) **DOI:10.1016/j.desal.2013.08.006**

[5] Touileb, K., Hedhibi, A. C., Djoudjou, R., Ouis, A., Bensalama, A., Ibrahim, A., Ahmed, M.M. Mechanical, microstructure, and corrosion characterization of dissimilar austenitic 316L and duplex 2205 stainless-steel ATIG welded joints. *Materials* 15 2470 (2022), **DOI:10.3390/ma15072470**

[6] Xiong, J., Tan, M.Y., Forsyth, M. (2013). The corrosion behaviors of stainless steel weldments in sodium chloride solution observed using a novel electrochemical measurement approach. *Desalination*, 327 39-45 **DOI:10.1016/j.desal.2013.08.006**

[7] Mohamed, A.Y., Mohamed, A.H.A., Abdel Hamid, Z., Farahat, A.I.Z., El-Nikhaily, A.E. Effect of heat treatment atmospheres on microstructure evolution and corrosion resistance of 2205 duplex stainless steel weldments. *Sci Rep* 13 4592 (2023) **DOI:10.1038/s41598-023-31803-5**

[8] Rao, P., Mulky, L. An overview of microbiologically influenced corrosion on stainless steel. *Chem Bio Eng Rev* 10 829-840 (2023) **DOI:10.1002/cben.202300001**

[9] Raj, S., Biswas, P. Experimental investigation of the effect of induction preheating on the microstructure evolution and corrosion behaviour of dissimilar FSW (IN718 and SS316L) joints. *J Manuf Process* 95 143-159 (2023) **DOI:10.1016/j.jmapro.2023.04.021**

[10] Okonkwo, B.O., Ming, H., Li, Z., Li, L., Chen, Y., Peng, J., Wang, J. Insight into the galvanic corrosion behaviour of low alloy steel A508/309 L/308 L stainless steel dissimilar metal weld at different temperatures. *Mater Today Comm* 38 107963. (2024) **DOI:10.1016/j.mtcomm.2023.107963**

[11] Liao, T., Zhang, X., Yang, H., Zhou, P., & Chen, F. Microstructural evolution and micro-corrosion behaviour of flash-welded U71Mn Joints as a function of post-weld heat treatment. *Materials* 16 5437 (2023) **DOI:10.3390/ma16155437**

[12] Vucko, F., Nazarov, A., Helbert, V., Thierry, D., Pelletier, S., Pablo, H., et al. Wet corrosion of incinerators under chloride deposits: insights from experimental study on stainless steels and nickel-based alloy weldments. *Corros Sci* 112220 (2024) **DOI:10.1016/j.corsci.2024.112220**

[13] Costa, E.M., Dedavid, B.A., Santos, C.A., Lopes, N.F., Fraccaro, C., Pagartanidis, T., Lovatto, L.P. Crevice corrosion on stainless steels in oil and gas industry: A review of techniques for evaluation, critical environmental factors and dissolved oxygen. *Eng Fail Anal* 144 106955 (2023) **DOI:10.1016/j.engfailanal.2022.106955**

[14] Singh Raman, R.K., Siew, W.H. Microstructures and corrosion/localised corrosion of stainless steels, incoloy and their weldments in nitrite-containing chloride environments. *Materials* 17 1336 (2024) **DOI:10.3390/ma17061336**

[15] Tahaei, A., Vanani, B.B., Abbasi, M., Garagnani, G.L. A comparison of microstructure and mechanical characteristics correlation of the joint specimens for duplex stainless steel UNS S32304 and super-duplex stainless steel UNS S32750: The role of post-weld heat treatment. *P I Mech Eng L-J Mat* (2024) **DOI:10.1177/14644207241233150**

[16] Tuz, L., Sokołowski, Ł., Stano, S. Effect of post-weld heat treatment on microstructure and hardness of laser beam welded 17-4 PH stainless steel. *Materials* 16 1334 (2023) **DOI:10.3390/ma16041334**

[17] Khan, M., Dewan, M.W., Sarkar, M.Z. Effects of welding technique, filler metal and post-weld heat treatment on stainless steel and mild steel dissimilar welding joint. *J Manuf Process* 64 1307-1321 (2021) **DOI:10.1016/j.jmapro.2021.02.058**

[18] Hung, C.H., Chen, W.T., Sehhat, M.H., Leu, M.C. The effect of laser welding modes on mechanical properties and microstructure of 304L stainless steel parts fabricated by laser-foil-printing additive manufacturing. *Int J Adv Manuf Tech* 112 867-877 (2021) **DOI:10.1007/s00170-020-06402-7**

[19] ASTM E8M-04. Standard Test Methods for Tension Testing of Metallic Materials [Metric Units]. American Society for Testing and Materials (ASTM) (2004) West Conshohocken **DOI:10.1520/E0008_E0008M-22**

[20] Lei, Z., Cao, H., Cui, X., Jin, G., Xu, K., Jiang, B., Huang, R. (2022). Analysis of welding solidification crack in narrow gap laser welding of high-strength steel. *Int J Adv Manuf Tech* 119, 4177-4190 **DOI:10.1007/s00170-022-08659-6**

[21] Dong, H., Yang, J., Li, Y., Xia, Y., Hao, X., Li, P., Lei, M. Evolution of interface and tensile properties in 5052 aluminum alloy/304 stainless steel rotary friction welded joint after post-weld heat treatment. *J Manuf Process* 51, 142-150 (2020) **DOI:10.1016/j.jmapro.2020.01.038**

[22] Köse, C., Topal, C. Effect of heat input and post-weld heat treatment on surface, texture, microstructure, and mechanical properties of dissimilar laser beam welded AISI 2507 super duplex to AISI 904L super austenitic stainless steels. *J Manuf Process* 73 861-894 (2022) **DOI:10.1016/j.jmapro.2021.11.040**

[23] Fontinha, I.R., Eustáquio, E. Influence of exposure conditions and particulate deposition on anodized aluminum corrosion. *Corr Mater Degrad* 3 770-786 (2022) **DOI:10.3390/cmd3040040**

[24] Hu, S., Liu, R., Liu, L., Cui, Y., Wang, F. Influence of temperature and hydrostatic pressure on the galvanic corrosion between 90/10 Cu-Ni and AISI 316L stainless steel. *J Mater Res Tech* 13 1402-1415 (2021) **DOI:10.1016/j.jmrt.2021.05.067**

[25] Wang, X, Chen, X., Han, Z., Li, C. Wang, Q. Stress corrosion cracking behavior of 2205 duplex stainless steel in 3.5% NaCl solution with sulfate reducing bacteria. *J Chinese Soc Corr Prot* 41 43-50 (2021) **DOI:10.1016/S0010-938X(99)00105-5**

[26] Dak, G., Sirohi, S., Pandey, C. Study on microstructure and mechanical behavior relationship for laser-welded dissimilar joint of P92 martensitic and 304L austenitic steel. *Int J Press Vess Pip* 196 104629 (2022) **DOI:10.1016/j.ijpvp.2022.104629**

[27] Bozeman, S.C. *The Processing and Microstructures of 309L Stainless Steel Clad onto Carbon Steel with Wire-fed Directed Energy Deposition.* Msc Thesis, Oregon State University, Corvallis (2022).

[28] Parvizi, R. *Electrochemical and interfacial characterisation of localised corrosion at heterogeneous structures in AA2024*. PhD Thesis, Deakin University, Victoria, (2022)

[29] Li, J., Jia, C., Gao, S., Guo, L. (2024). Experimental and numerical study on axial compression behavior of slender CFST columns with localized pitting corrosion damage. *Constr Build Mater* 414 134858 **DOI:10.1016/j.conbuildmat.2023.134858**

[30] Singh, J., Shahi, A.S. Microstructure and corrosion behavior of duplex stainless steel electron beam welded joint. *J Mater Sci* 57 9454-9479 (2022) **DOI:10.1007/s10853-022-07241-5**

[31] Jiang, L., Zhang, Z., Fu, H., Huang, S., Zhuang, D., Xie, J. Corrosion behavior and mechanism of Al-Zn-Mg-Cu alloy based on the characterization of the secondary phases. *Mater Charact* 189, 111974 (2022) **DOI:10.2139/ssrn.4009387**

[32] Örnek, C., Davut, K., Kocabaş, M., Bayatlı, A., Ürgen, M. Understanding corrosion morphology of duplex stainless steel wire in chloride electrolyte. Corr Mater Degr 2 397-411 (2021) **DOI:10.3390/cmd2030021**

[33] Hammood, A.S., Esmailzadeh, M., Hosseini, S.N., Karimi, S., Calliari, I., Pezzato, L., Brittain, R. Effect of friction stir welding parameters on microstructure and corrosion behavior of 2101 duplex stainless steel in simulated body fluid. *Int J Pr Eng Man-GT* 10 327-337 (2023) **DOI:10.1007/s40684-022-00440-0**

[34] Amiri, E., Ostovan, F., Toozandehjani, M., Shafiei, E., Mohamed, I.F. Study and selection of most appropriate filler rod for GTAW of S32750 super duplex steel joints: A comprehensive study on microstructural, mechanical and corrosion properties. *Mater Chem Phys* 270 124839 (2021) **DOI:10.1016/j.matchemphys.2021.124839**

[35] Wang, Q., Zhang, Q., Zheng, H., Liu, L., Wu, X., Zhao, C Li, X. (2023). Insight into anti-corrosion behavior of protein extract as eco-friendly corrosion inhibitor. *Sust Chem Pharm* 34 101177 **DOI:10.1016/j.scp.2023.101177**

[36] Örnek, C., Davut, K., Kocabaş, M., Bayatlı, A., Ürgen, M. Understanding corrosion morphology of duplex stainless steel wire in chloride electrolyte. *Corr Mater Degr* 2 397-411. (2021) **DOI:10.3390/cmd2030021**

[37] Lovše, A., Skale, S., Vojvodić-Tuma, J. Evaluation of the Condition of the Bottom of the Tanks for Petroleum Products-Forecast of the Remaining Operating Life. *Stroj Vestn-J Mech E*, 70, 282-292. (2024) **DOI:10.5545/sv-jme.2023.682**

[38] Calabrese, L., Galeano, M., Proverbio, E. Data mining applied to the electrochemical noise technique in the time/frequency domain for stress corrosion cracking recognition. *Corr Mater Degr* 4 659-679 (2023) **DOI:10.3390/cmd4040034**

Acknowledgement

The authors would like to thank National Central Instrumentation Facility, Tamil Nadu, India for assistance in microstructural evaluation and M/s.Vikram Engineering Industry, Trichy, Tamil Nadu, India for assistance in welding and heat treatment studies.

Received 2024-07-03, revised 2024-09-29, accepted 2024-11-05,
Original Scientific Paper.

Data availability *The data supporting the study's findings are included in the paper.*

Author contribution *Mahadevan Govindasamy contributed to data curation, drafting; Lloyd Jenner Mangalakaran Joseph Manuel contributed to analysis; and Senthilkumar Thamilkolunthu contributed to implementation of the work.*

Študija korozije neenakih zvarov AISI2205 in AISI310 po varjenju z elektrokemično analizo šuma

Povzetek *Korozijsko obnašanje neenakih zvarov nerjavnih jekel AISI310 in AISI2205v 5-odstotni raztopini kalcijevega klorida pri 50 °C je bilo raziskano pod tremi pogoji: kot varjeno, z nižjo toplotno obdelavo po varjenju pri 800 °C in z višjo toplotno obdelavo po varjenju pri 1000 °C. Mikrostrukturna analiza je pokazala izrazito jamasto korozijopri varjenem vzorcu, pri čemer so bile širine jamic med 270 µm in 360 µm. Vzorec z nižjo toplotno obdelavo je imel večje vdolbine (310 µm do 370 µm), medtem ko je pri vzorcu, ki je bil toplotno obdelan višje, opaziti homogeno korozijo z zaščitno oksidno prevleko. Najvišjo stopnjo korozije je imel varjeni vzorec, sledil mu je nizko-toplotno obdelani vzorec z zmerno stopnjo, najnižjo stopnjo korozije pa je imel visoko-toplotno obdelani vzorec. Gostote korozijskega toka so bile* $5{,}26 \times 10^{-3}$ *mA/cm²,* $4{,}6 \times 10^{-4}$ *mA/cm²* *oziroma* $1{,}4 \times 10^{-4}$ *mA/cm². Elektrokemične meritve šuma so potrdile te ugotovitve, pri čemer je vzorec, ki je bil obdelan z višjo toplotno obdelavo, pokazal zanemarljivo lokalizirano korozijo in homogeno korozijsko obnašanje.*

Ključne besede *AISI2205, AISI310, korozija, elektrokemijska impedančna spektroskopija,* $CaCl_2$